

# Distributed model building and recursive integration for big spatial data modeling

Emily C. Hector\*

Department of Statistics, North Carolina State University

Ani Eloyan

Department of Biostatistics, Brown University

## Abstract

Motivated by the important need for computationally tractable statistical methods in high dimensional spatial settings, we develop a distributed and integrated framework for estimation and inference of Gaussian model parameters with ultra-high-dimensional likelihoods. We propose a paradigm shift from whole to local data perspectives that is rooted in distributed model building and integrated estimation and inference. The framework's backbone is a computationally and statistically efficient integration procedure that simultaneously incorporates dependence within and between spatial resolutions in a recursively partitioned spatial domain. Statistical and computational properties of our distributed approach are investigated theoretically and in simulations. The proposed approach is used to extract new insights on autism spectrum disorder from the Autism Brain Imaging Data Exchange.

*Keywords: Divide-and-conquer, Generalized method of moments, Nearest-neighbour Gaussian process, Neuroimaging, Optimal estimating functions.*

## 1 Introduction

With recent developments in large-scale imaging and satellite data collection, traditional spatial data analysis techniques that fit a model on the entire spatial domain are rendered computationally intractable. On the other hand, leveraging the rich information available with spatially dependent outcomes by incorporating dependence between all observations is crucial to actualizing the promise of new scientific discoveries with big spatial data. Many methods for balancing these two fundamental necessities have been proposed, but increasing data sizes continuously test the limits of existing methodology. To develop appropriate new methods that withstand the test of future data growth, we propose a paradigm shift from

---

\*Hector was supported by a grant from the National Science Foundation (DMS2152887) and a Faculty Research and Professional Development Award from North Carolina State University.

whole to local data perspectives that is rooted in distributed model building and integrated estimation and inference.

Gaussian process models provide a large and flexible class of models that are widely used in spatial data modeling (Cressie, 1993; Schabenberger and Gotway, 2004; Banerjee et al., 2014; Cressie and Wikle, 2015). Consider the true spatial process  $\{y(\mathbf{s}) : \mathbf{s} \in \mathcal{D}\}$ , or  $y(\cdot)$ , on a continuous domain  $\mathcal{D} \subset \mathbb{R}^d$ ,  $d \in \mathbb{N}$ , and suppose  $y(\cdot)$  has been observed at a set  $\mathcal{S}$  of  $S$  locations for  $i = 1, \dots, N$  independent samples. The joint distribution of  $y_i(\mathcal{S})$  is assumed multivariate Gaussian and known up to a vector of parameters of interest  $\boldsymbol{\theta}$ . Without further modeling assumptions or dimension reduction techniques, maximum likelihood estimation and inference for  $\boldsymbol{\theta}$  generally has memory and computational complexity  $O(NS^2)$  and  $O(NS^3)$  respectively due to the  $S$ -dimensional covariance matrix. For inference on  $\boldsymbol{\theta}$  when  $S$  is large, the crux of the problem is to adequately model the spatial dependence without storing or inverting a large covariance matrix.

This problem has received considerable attention in the literature. Solutions include, for example, the composite likelihood (CL) (Lindsay, 1988; Varin et al., 2011) and the related nearest-neighbour Gaussian process (Datta et al., 2016a,b; Finley et al., 2019), spectral methods (Fuentes, 2007), tapered covariance functions (Furrer et al., 2006; Kaufman et al., 2008; Stein, 2013; Furrer et al., 2016), separable covariance structures (Genton, 2007; Gneiting et al., 2007), low-rank approximations (Zimmerman, 1989; Higdon, 2002; Lemos and Sansó, 2009; Cressie and Johannesson, 2008; Kang and Cressie, 2011; Katzfuss and Cressie, 2011; Banerjee et al., 2008; Finley et al., 2009; Nychka et al., 2015; Lindgren et al., 2011), and combinations thereof (Sang and Huang, 2012). See the excellent reviews of Sun et al. (2011); Bradley et al. (2016); Heaton et al. (2019); Liu et al. (2020) for additional references. Stein (2007, 2013); Stein et al. (2013) detail shortcomings of the aforementioned methods, which are primarily related to loss of statistical efficiency due to simplification of the covariance matrix or its inverse. Moreover, these methods remain computationally burdensome when  $S$  is truly massive, e.g.  $S \gtrsim 10^6$ .

The proposed methods are motivated by the investigation of differences in brain functional organization between children with Autism Spectrum Disorder (ASD) and their typically developing peers. The Autism Brain Imaging Data Exchange (ABIDE) neuroimaging study of resting-state functional Magnetic Resonance Imaging (rfMRI) provides a large database for studying brain functional organization in those with ASD. ABIDE aggregated and publicly shared neuroimaging data on participants with ASD and neurotypical controls from 16 international imaging sites. rfMRI measures blood oxygenation in the absence of a stimulus or task and characterizes intrinsic brain activity (Fox and Raichle, 2007). Relationships between activation of brain regions of interest (ROIs) during rest can be characterized by functional connectivity between ROIs using rfMRI data. Functional connectivity between two ROIs is typically estimated from the subject-specific correlation constructed from the rfMRI time series (Wang et al., 2010; He et al., 2009). In this pipeline, to avoid the computational burden of estimating a connectivity matrix with  $O(v_1 v_2)$  entries, where  $v_r$  is the number of voxels in ROI  $r$ , the rfMRI time series is averaged across voxels in each ROI before computing the cross-ROI correlation. This standard approach is substantially underpowered to detect small effect sizes. While ABIDE data have led to some evidence that ASD can be broadly characterized as a brain dysconnection syndrome, findings have varied across studies (Ha et al., 2015; Uddin et al., 2013; Lynch et al., 2013; Rahko et al., 2016; Alaerts

et al., 2014; Di Martino et al., 2013, 2014; Wolff et al., 2018). Hence, computationally and statistically efficient estimation of robust functional connectivity maps is essential in identifying dysconnections in ASD and is the main motivation for this study. In this paper, we show how to estimate the effect of ASD on over 3 million cross-ROI correlations in half an hour, and demonstrate the improved statistical power afforded by our more granular estimation approach leading to new insights in understanding differences in brain functional connectivity in ASD.

We propose a new distributed and integrated framework for big spatial data analysis. We consider a recursive partition of the spatial domain  $\mathcal{S}$  into  $M$  nested resolutions with disjoint sets of spatial observations at each resolution, and build local, fully specified distributed models in each set at the highest spatial resolution. The main technical difficulty arises from integrating inference from these distributed models over two levels of dependence: between sets in each resolution, and between resolutions. Simultaneously incorporating dependence between all sets and resolutions results in a high-dimensional dependence matrix that is computationally prohibitive to handle. The critical contribution of this paper is a recursive estimator that integrates inference over all sets and resolutions by alternating between levels of dependence at each integration step. We also propose a sequential integrated estimator that is asymptotically equivalent to the recursive integrated estimator. In very high-dimensional settings, this estimator further reduces the computational burden of recursively integrating over multiple resolutions. The resulting Multi-Resolution Recursive Integration (MRRI) framework is flexible, statistically efficient, and computationally scalable through its formulation in the MapReduce paradigm.

The rest of this paper is organized as follows. Section 2 establishes the formal problem setup, and describes the distributed model building step and the recursive integration scheme for the proposed MRRI framework. Section 3 establishes asymptotic properties of the recursive integrated estimator. Section 4 describes the asymptotically equivalent sequential integration scheme. Section 5 evaluates the proposed frameworks with simulations. Section 6 presents a neuroimaging application with the analysis of data from ABIDE. Proofs, additional simulations, ABIDE information and an R package are provided in the supplement.

## 2 Recursive Model Integration Framework

### 2.1 Problem set-up

We assume that  $y(\cdot) = \alpha(\cdot) + \epsilon(\cdot)$ , where  $\alpha(\cdot)$  characterizes the spatial variations and  $\epsilon(\cdot)$  is an independent normally distributed measurement error with mean 0 and variance  $\sigma^2$  independent of  $\alpha(\cdot)$ . Suppose  $y(\cdot)$  has been observed at a set  $\mathcal{S} = \{\mathbf{s}_j\}_{j=1}^S$  of locations for  $\{y_i(\mathcal{S})\}_{i=1}^N$  independently, with corresponding observations  $\mathbf{X}_i(\mathcal{S})$  on  $q$  explanatory variables  $\mathbf{X}(\mathbf{s}) \in \mathbb{R}^q$ . In the motivating data analysis of Section 6,  $y_i(\mathcal{S})$  is a measure of the functional connectivity between two regions of interest for each ABIDE participant  $i$ . Specifically, we define  $y_i(\mathbf{s}_j)$  as the correlation between the rfMRI time series at voxels  $\mathbf{v}_{j_1}$  and  $\mathbf{v}_{j_2}$ , where  $\mathbf{v}_{j_1}$  and  $\mathbf{v}_{j_2}$  are voxels in the left and right precentral gyri respectively. Then,  $\mathcal{S}$  is the set of  $S$  voxel-pair locations  $\mathbf{s}_j = \{\mathbf{v}_{j_1}, \mathbf{v}_{j_2}\}$ . The left and right precentral gyri are visualized in Figure 1. Explanatory variables  $\mathbf{X}_i(\mathbf{s}) = \mathbf{X}_i$  considered in Section 6 consist of an intercept,

ASD status, age, sex and the age by ASD status interaction.

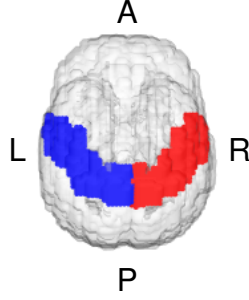


Figure 1: Left (blue) and right (red) precentral gyri.

We assume that  $\alpha(\cdot) \sim GP[\mu\{\cdot; \mathbf{X}(\cdot), \boldsymbol{\beta}\}, C_\alpha(\cdot, \cdot; \boldsymbol{\gamma})]$  is a Gaussian Process with mean  $\mu\{\cdot; \mathbf{X}(\cdot), \boldsymbol{\beta}\}$  and stationary positive-definite covariance function  $C_\alpha(\cdot, \cdot; \boldsymbol{\gamma})$ . We further assume that  $\mu\{\mathcal{S}; \mathbf{X}_i(\mathcal{S}), \boldsymbol{\beta}\}$  is known up to a  $q$ -dimensional vector of parameters  $\boldsymbol{\beta}$ , and  $C_\alpha(\mathcal{S}, \mathcal{S}; \boldsymbol{\gamma})$  is known up to a  $p_\gamma$ -dimensional vector of parameters,  $\boldsymbol{\gamma}$ :  $C_\alpha(\mathbf{s}_1, \mathbf{s}_2; \boldsymbol{\gamma}) = \text{Cov}\{y(\mathbf{s}_1), y(\mathbf{s}_2)\}$ . We let  $\boldsymbol{\theta} = (\boldsymbol{\beta}, \boldsymbol{\gamma}, \sigma^2)$  the  $p$ -dimensional vector parameter of interest,  $p = p_\gamma + q + 1$ , which includes the “nugget effect”  $\sigma^2$ . The distribution of one sample,  $y_i(\mathcal{S}) \sim \mathcal{N}[\mu\{\mathcal{S}; \mathbf{X}_i(\mathcal{S}), \boldsymbol{\beta}\}, \mathbf{C}(\mathcal{S}, \mathcal{S}; \boldsymbol{\gamma}, \sigma^2)]$ , is an  $S$ -variate Gaussian distribution with mean  $\mu\{\mathcal{S}; \mathbf{X}_i(\mathcal{S}), \boldsymbol{\beta}\}$  and covariance matrix  $\mathbf{C}(\mathcal{S}, \mathcal{S}; \boldsymbol{\gamma}, \sigma^2) = \{C_\alpha(\mathbf{s}_r, \mathbf{s}_t; \boldsymbol{\gamma})\}_{r,t=1}^{S,S} + \text{diag}(\sigma^2)_{s=1}^S$ . When  $S$  is large ( $S \gtrsim 10^6$ ), the optimization of the likelihood is computationally infeasible. To overcome this difficulty, we borrow ideas from the composite likelihood (CL), multi-resolution approximations (MRA) and generalized method of moments (GMM) to propose a new distributed model building and integration framework.

## 2.2 Recursive Integration Framework

### 2.2.1 A Shift from Whole to Local Data Perspectives

The core philosophy of the CL approach is to divide  $\mathcal{S}$  into  $K$  (overlapping) subsets, to build well-specified local models on the  $K$  subsets, and to integrate them using working independence assumptions. The literature on CL in spatial and spatiotemporal statistics is rich (Vecchia, 1988; Curriero and Lele, 1999; Heagerty and Lele, 1998; Stein et al., 2004; Li and Lin, 2006; Bevilacqua et al., 2010, 2012; Bai et al., 2012). Block CL approaches construct likelihoods for small blocks of observations (Caragea and Smith, 2007; Eidsvik et al., 2014; Rulli  re et al., 2018). Optimally weighted composite likelihood methods are more statistically efficient (Cessie and van Houwelingen, 1994; Nott and Ryd  n, 1999; Kuk and Nott, 2000; Kuk, 2007; Joe and Lee, 2009; Zhao and Joe, 2009), but more computationally intensive. The CL is attractive because it offers a trade-off between statistical and computational efficiencies, and the maximum CL estimator is consistent and asymptotically normal under mild regularity conditions (Cox and Reid, 2004).

The main difficulty in the construction of the CL is the choice of  $K$ , which regulates both the number and the dimensionality of the marginal densities. Generally, large  $K$  is preferred as it alleviates the modeling difficulties and computational burden associated with specifying and evaluating multivariate densities. Large  $K$ , however, can result in the evaluation of a

large number of low-dimensional marginals, which is computationally expensive and results in loss of efficiency. When  $S$  is truly large, the trade-off is a lose-lose scenario where no choice of  $K$  is adequately statistically or computationally efficient, since the number of marginals is large and their dimension remains high. To achieve both a small number of sets and low-dimensional sets, we propose a recursive partition of  $\mathcal{S}$  into multiple resolutions, with multiple sets at each resolution.

This idea is, at first blush, similar to MRA models (Johannesson et al., 2007; Nychka et al., 2015; Katzfuss, 2017; Katzfuss and Gong, 2020; Appel and Pebesma, 2020), but with a crucial difference: we build local models at the highest resolution and recursively integrate inference from the highest to the lowest resolution. We propose to first model local structures at high resolutions and then to integrate these models for a hierarchical description of the data from the highest to the lowest resolutions. Unlike MRA models, we incorporate dependence within all spatial resolutions using the generalized method of moments (GMM) (Hansen, 1982) framework.

The GMM provides an intuitive mechanism for incorporating dependence between local models. It formulates a weighted quadratic form of estimating functions and minimizes this form in a similar spirit to the minimization of the negative log-likelihood. It is well known that the sample covariance of the estimating functions is an optimal choice of the weight matrix. Recently, Hector and Song (2021, 2020, 2022); Manschot and Hector (2022); Hector and Reich (2023) proposed closed-form meta-estimators for integrating estimators from dependent analyses that are asymptotically as statistically efficient as the optimal GMM estimators but that avoid computationally expensive iterative minimization of the GMM objective function. Extending this framework to recursively partitioned spatially dependent observations, however, leads to inversion of a dependence matrix for all sets of observations that is unfortunately high-dimensional, negating the gain in computation afforded by the partition. Substantial additional thought is required to develop a recursive integration scheme for dependent estimators within and across spatial resolutions. We propose a new weighting scheme based on optimal estimating function theory (Heyde, 1997) to optimally weight GMM estimating functions and reduce their dimension for computationally tractable recursive integration of dependent models.

### 2.2.2 Partitioning the Spatial Domain

Let  $\otimes 2$  denote the outer product of a vector with itself, namely  $\mathbf{a}^{\otimes 2} = \mathbf{a}\mathbf{a}^\top$ . We adopt the notation of Katzfuss (2017) to describe the recursive partitioning of  $\mathcal{S}$ . Denote  $\mathcal{A}_0 = \mathcal{S}$  and partition  $\mathcal{S}$  into  $K_1$  (disjoint) regions  $\{\mathcal{A}_1, \dots, \mathcal{A}_{K_1}\}$  that are again partitioned into  $K_2$  (disjoint) subregions  $\{\mathcal{A}_{k_1 1}, \dots, \mathcal{A}_{k_1 K_2}\}_{k_1=1}^{K_1}$ , and so on up to level  $M$ , i.e.

$$\mathcal{A}_{k_1 \dots k_{m-1}} = \cup_{k_m=1, \dots, K_m} \mathcal{A}_{k_1 \dots k_{m-1} k_m}, \quad k_{m-1} \in \{1, \dots, K_{m-1}\}, \quad m = 0, \dots, M,$$

where  $K_0 = 1$ . For completeness, let  $k_0 = 0$ . Figure 2 illustrates an example of a recursive partition of observations on a two-dimensional spatial domain for  $M = 2$  resolutions. For resolution  $m \in \{1, \dots, M\}$ , denote  $S_{k_1 \dots k_m}$  the size of  $\mathcal{A}_{k_1 \dots k_m}$ , with  $S_0 = S$ .  $M$  and  $K_m$  should be chosen so that  $S_{k_1 \dots k_M}$  and  $K_m, m = 1, \dots, M$  are relatively small compared to  $S_0$ . The literature is replete with methods for choosing partitions for Gaussian processes; see

Heaton et al. (2019) for an excellent review. In the data analysis of Section 6, we partition the set of voxel-pair locations  $\mathcal{S}$  based on nearest neighbours with  $M = 7$  resolutions.

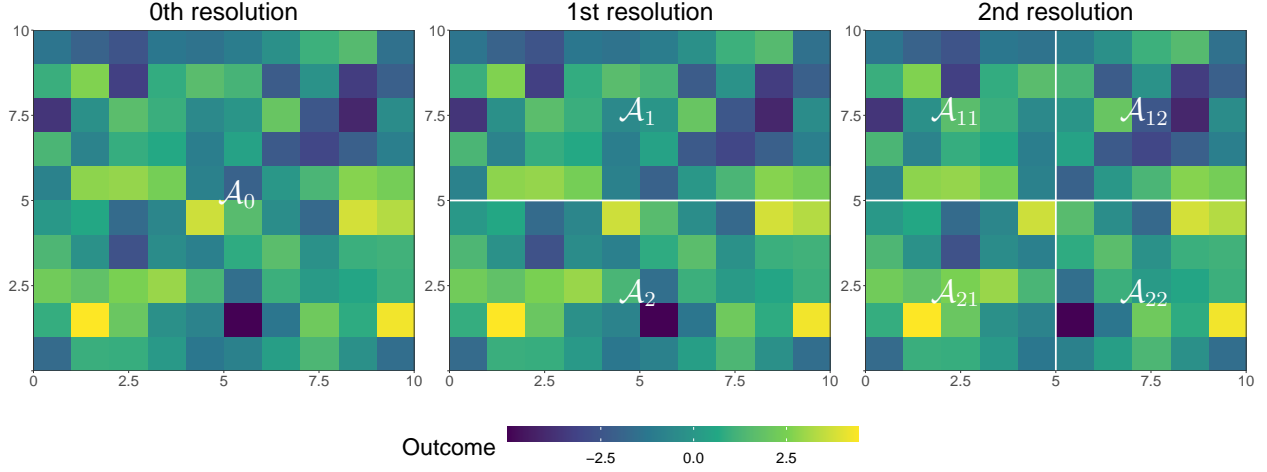


Figure 2: Example partition of observations on a two-dimensional spatial domain,  $M = 2$ .

### 2.2.3 Local Model Specification

At resolution  $M$  for  $k_M \in \{1, \dots, K_M\}$ , the likelihood of the data in set  $\mathcal{A}_{k_1 \dots k_M}$  is given by  $y_i(\mathcal{A}_{k_1 \dots k_M}) \sim \mathcal{N}[\mu\{\mathcal{A}_{k_1 \dots k_M}; \mathbf{X}_i(\mathcal{A}_{k_1 \dots k_M}), \boldsymbol{\beta}\}; \mathbf{C}(\mathcal{A}_{k_1 \dots k_M}, \mathcal{A}_{k_1 \dots k_M}; \boldsymbol{\gamma}, \sigma^2)]$ . The covariance function  $\mathbf{C}$  can be chosen as best suits the data using covariograms; see Cressie (1993) for examples. We model the mean of the spatial process through  $\mu\{\mathcal{A}_{k_1 \dots k_M}; \mathbf{X}_i(\mathcal{A}_{k_1 \dots k_M}), \boldsymbol{\beta}\} = \mathbf{X}_i^\top(\mathcal{A}_{k_1 \dots k_M})\boldsymbol{\beta}$ . Due to the recursive partitioning,  $S_{k_1 \dots k_M}$  is small and the full likelihood tractable. Denote the log-likelihood of the data in  $\mathcal{A}_{k_1 \dots k_M}$  as  $\ell_{k_1 \dots k_M}(\boldsymbol{\theta})$  and the score function as  $\boldsymbol{\Psi}_{k_1 \dots k_M}(\boldsymbol{\theta}) = \nabla_{\boldsymbol{\theta}} \ell_{k_1 \dots k_M}(\boldsymbol{\theta}) = \sum_{i=1}^N \boldsymbol{\psi}_{i, k_1 \dots k_M}(\boldsymbol{\theta})$ . The maximum likelihood estimator (MLE)  $\hat{\boldsymbol{\theta}}_{k_1 \dots k_M}$  of  $\boldsymbol{\theta}$  is obtained by maximizing the log-likelihood, or equivalently solving  $\boldsymbol{\Psi}_{k_1 \dots k_M}(\boldsymbol{\theta}) = \mathbf{0}$ .

## 2.3 Recursive Model Integration

### 2.3.1 Generalized Method of Moments Approach

Now that we have modeled the local structures, we wish to recursively integrate the models at each resolution. For  $m = M, \dots, 0$ , let  $k_m \in \{1, \dots, K_m\}$  denote the index for the sets at resolution  $m$ . We describe a recursive GMM approach that consists of re-estimating  $\boldsymbol{\theta}$  at each resolution  $M - 1$  based on an optimally weighted form of the generalized method of moments equation from the higher resolution  $M$ .

To formulate the recursive definition of the estimating function approach, consider resolution  $M - 1$ . At resolution  $M - 1$ , we define  $K_{M-1}$  estimating functions based on the score

functions from resolution  $M$ :

$$\begin{aligned}\psi_{i,k_1\dots k_{M-1}}(\boldsymbol{\theta}) &= \{\psi_{i,k_1\dots k_{M-1}k_M}(\boldsymbol{\theta})\}_{k_M=1}^{K_M} \in \mathbb{R}^{pK_M}, \quad k_m = 1, \dots, K_{M-1}, \\ \Psi_{k_1\dots k_{M-1}}(\boldsymbol{\theta}) &= \{\Psi_{k_1\dots k_{M-1}k_M}(\boldsymbol{\theta})\}_{k_M=1}^{K_M} \in \mathbb{R}^{pK_M}, \quad k_{M-1} = 1, \dots, K_{M-1}.\end{aligned}\quad (1)$$

Clearly, the estimating function  $\Psi_{k_1\dots k_{M-1}}(\boldsymbol{\theta})$  over-identifies  $\boldsymbol{\theta} \in \mathbb{R}^p$ , i.e. there are several estimating functions for each parameter. Following Hansen (1982)'s GMM, we propose to minimize the quadratic form  $Q_{k_1\dots k_{M-1}}(\boldsymbol{\theta}) = \Psi_{k_1\dots k_{M-1}}^\top(\boldsymbol{\theta})\mathbf{W}\Psi_{k_1\dots k_{M-1}}(\boldsymbol{\theta})$ , with a positive semi-definite weight matrix  $\mathbf{W}$ . Hansen (1982) showed that the optimal choice of  $\mathbf{W}$  is the inverse of the covariance of  $\Psi_{k_1\dots k_{M-1}}(\boldsymbol{\theta})$ . The covariance can be consistently estimated by  $N^{-1}\mathbf{V}_{k_1\dots k_{M-1}}(\hat{\boldsymbol{\theta}}_{k_1\dots k_M})$  with

$$\mathbf{V}_{k_1\dots k_{M-1}}(\hat{\boldsymbol{\theta}}_{k_1\dots k_M}) = \sum_{i=1}^N \{\psi_{i,k_1\dots k_{M-1}}(\hat{\boldsymbol{\theta}}_{k_1\dots k_M})\}^{\otimes 2}, \quad (2)$$

and  $\psi_{i,k_1\dots k_{M-1}}(\hat{\boldsymbol{\theta}}_{k_1\dots k_M}) = \{\psi_{i,k_1\dots k_M}(\hat{\boldsymbol{\theta}}_{k_1\dots k_{M-1}k_M})\}_{k_M=1}^{K_M}$ . The matrix  $N^{-1}\mathbf{V}_{k_1\dots k_{M-1}}(\hat{\boldsymbol{\theta}}_{k_1\dots k_M})$  estimates dependence between score functions from all sets in  $\mathcal{A}_{k_1\dots k_{M-1}}$  and thus captures dependence between sets  $\{\mathcal{A}_{k_1\dots k_M}\}_{k_M=1}^{K_M}$ . This choice is optimal in the sense that

$$\hat{\boldsymbol{\theta}}_{GMM} = \arg \min_{\boldsymbol{\theta}} Q_{k_1\dots k_{M-1}}^*(\boldsymbol{\theta}) = \arg \min_{\boldsymbol{\theta}} \Psi_{k_1\dots k_{M-1}}^\top(\boldsymbol{\theta})\mathbf{V}_{k_1\dots k_{M-1}}^{-1}(\hat{\boldsymbol{\theta}}_{k_1\dots k_M})\Psi_{k_1\dots k_{M-1}}(\boldsymbol{\theta}) \quad (3)$$

has minimum variance among estimators  $\arg \min_{\boldsymbol{\theta}} Q_{k_1\dots k_{M-1}}(\boldsymbol{\theta})$  for all possible choices of  $\mathbf{W}$ , a property termed ‘‘Hansen optimality’’. The computation of  $Q_{k_1\dots k_{M-1}}^*(\boldsymbol{\theta})$  in (3) requires inversion of the  $(pK_M) \times (pK_M)$  dimensional matrix  $\mathbf{V}_{k_1\dots k_{M-1}}^{-1}(\hat{\boldsymbol{\theta}}_{k_1\dots k_M})$ , substantially smaller than inverting the  $(pS_{k_1\dots k_{M-1}}) \times (pS_{k_1\dots k_{M-1}})$  dimensional matrix in the direct evaluation of the likelihood on set  $\mathcal{A}_{k_1\dots k_{M-1}}$ . This yields a faster computation than a full likelihood approach on  $\mathcal{A}_{k_1\dots k_{M-1}}$ . The iterative minimization in (3), however, can be time consuming because it requires computation of the score functions  $\Psi_{k_1\dots k_M}$  at each iteration.

In the spirit of Hector and Song (2021), a closed-form meta-estimator asymptotically equivalent to the GMM estimator  $\hat{\boldsymbol{\theta}}_{GMM}$  in (3) that is more computationally attractive is given by

$$\hat{\boldsymbol{\theta}}_{k_1\dots k_{M-1}} = \mathbf{J}_{k_1\dots k_{M-1}}^{-1}(\hat{\boldsymbol{\theta}}_{k_1\dots k_M})\mathbf{S}_{k_1\dots k_{M-1}}(\hat{\boldsymbol{\theta}}_{k_1\dots k_M})\mathbf{V}_{k_1\dots k_{M-1}}^{-1}(\hat{\boldsymbol{\theta}}_{k_1\dots k_M})\mathbf{T}_{k_1\dots k_{M-1}}(\hat{\boldsymbol{\theta}}_{k_1\dots k_M}), \quad (4)$$

where

$$\begin{aligned}\mathbf{S}_{k_1\dots k_{M-1}}(\hat{\boldsymbol{\theta}}_{k_1\dots k_M}) &= -\{\nabla_{\boldsymbol{\theta}}\Psi_{k_1\dots k_{M-1}}(\boldsymbol{\theta})|_{\boldsymbol{\theta}=\hat{\boldsymbol{\theta}}_{k_1\dots k_M}}\}^\top \in \mathbb{R}^{p \times pK_M}, \\ \mathbf{T}_{k_1\dots k_{M-1}}(\hat{\boldsymbol{\theta}}_{k_1\dots k_M}) &= \begin{Bmatrix} \mathbf{S}_{k_1\dots k_{M-1}1}^\top(\hat{\boldsymbol{\theta}}_{k_1\dots k_M})\hat{\boldsymbol{\theta}}_{k_1\dots k_{M-1}1} \\ \vdots \\ \mathbf{S}_{k_1\dots k_{M-1}K_M}^\top(\hat{\boldsymbol{\theta}}_{k_1\dots k_M})\hat{\boldsymbol{\theta}}_{k_1\dots k_{M-1}K_M} \end{Bmatrix} \in \mathbb{R}^{pK_M}, \\ \mathbf{J}_{k_1\dots k_{M-1}}(\hat{\boldsymbol{\theta}}_{k_1\dots k_M}) &= \mathbf{S}_{k_1\dots k_{M-1}}(\hat{\boldsymbol{\theta}}_{k_1\dots k_M})\mathbf{V}_{k_1\dots k_{M-1}}^{-1}(\hat{\boldsymbol{\theta}}_{k_1\dots k_M})\mathbf{S}_{k_1\dots k_{M-1}}^\top(\hat{\boldsymbol{\theta}}_{k_1\dots k_M}) \in \mathbb{R}^{p \times p}.\end{aligned}$$

In the Gaussian process model,  $\mathbf{S}_{k_1\dots k_{M-1}}(\hat{\boldsymbol{\theta}}_{k_1\dots k_M})$  can be efficiently computed by Bartlett's identity.



When updating to the next resolution  $M - 2$ , it is tempting to proceed again through the GMM approach and to stack estimating functions  $\{\Psi_{k_1 \dots k_{M-1}}\}_{k_{M-1}=1}^{K_{M-1}}$ . This would, however, result in a vector of over-identified estimating functions on  $\theta$  of dimension  $pK_{M-1}K_M$ , and therefore inversion of a  $(pK_{M-1}K_M) \times (pK_{M-1}K_M)$  dimensional covariance matrix. One can easily see how recursively proceeding this way would lead to the computationally prohibitive inversion of a  $(pK_1 \dots K_M) \times (pK_1 \dots K_M)$  dimensional matrix at resolution  $m = 0$ . To avoid this difficulty, we propose weights in the spirit of optimal estimating function theory.

### 2.3.2 Weighted Over-Identified Estimating Functions

We define new estimating functions at resolution  $m = M - 2, \dots, 0$  that optimally weight the estimating functions from resolution  $m + 1$ . Using optimal estimating function theory (Heyde, 1997), we define

$$\begin{aligned}\tilde{\psi}_{i,k_1 \dots k_{M-1}}(\theta) &= -\mathbf{S}_{k_1 \dots k_{M-1}}(\hat{\theta}_{k_1 \dots k_{M-1}}) \mathbf{V}_{k_1 \dots k_{M-1}}^{-1}(\hat{\theta}_{k_1 \dots k_{M-1}}) \psi_{i,k_1 \dots k_{M-1}}(\theta) \in \mathbb{R}^p \\ \tilde{\Psi}_{k_1 \dots k_{M-1}}(\theta) &= -\mathbf{S}_{k_1 \dots k_{M-1}}(\hat{\theta}_{k_1 \dots k_{M-1}}) \mathbf{V}_{k_1 \dots k_{M-1}}^{-1}(\hat{\theta}_{k_1 \dots k_{M-1}}) \Psi_{k_1 \dots k_{M-1}}(\theta) \in \mathbb{R}^p,\end{aligned}\tag{5}$$

where  $\mathbf{S}_{k_1 \dots k_{M-1}}^\top(\hat{\theta}_{k_1 \dots k_{M-1}})$  and  $\mathbf{V}_{k_1 \dots k_{M-1}}(\hat{\theta}_{k_1 \dots k_{M-1}})$  are recomputed so as to evaluate the sensitivity and variability at the estimator from resolution  $M - 1$ . This formulation can also be viewed as the optimal projection of the estimating function  $\Psi_{k_1 \dots k_{M-1}}(\theta)$  onto the parameter space of  $\theta$  (Heyde, 1997). Stacking  $\{\tilde{\Psi}_{k_1 \dots k_{M-1}}(\theta)\}_{k_{M-1}=1}^{K_{M-1}}$  yields  $\Psi_{k_1 \dots k_{M-2}}(\theta)$ , a  $pK_{M-1}$  dimensional vector of over-identifying estimating functions on  $\theta$ . Defining  $\mathbf{V}_{k_1 \dots k_{M-2}}(\hat{\theta}_{k_1 \dots k_{M-1}})$  the sample covariance of  $\Psi_{k_1 \dots k_{M-2}}(\theta)$  evaluated at  $\hat{\theta}_{k_1 \dots k_{M-1}}$ , one can again define the closed-form meta-estimator  $\hat{\theta}_{k_1 \dots k_{M-2}}$  in the fashion of (4). This requires inversion of a  $(pK_{M-1}) \times (pK_{M-1})$ -dimensional matrix, substantially smaller than inverting the  $S_{k_1 \dots k_{M-2}} \times S_{k_1 \dots k_{M-2}}$ -dimensional matrix in the full likelihood on set  $\mathcal{A}_{k_1 \dots k_{M-2}}$ .

### 2.3.3 Recursive Integration Procedure

The recursive integration procedure defined by updating through Sections 2.3.1 and 2.3.2 is summarized in the supplement. At resolution  $m = 0$ , we obtain  $\psi_{i,0}(\hat{\theta}_{k_1}) = \{\psi_{i,k_1}(\hat{\theta}_{k_1})\}_{k_1=1}^{K_1} \in \mathbb{R}^{pK_1}$ ,  $\Psi_0(\hat{\theta}_{k_1}) = \{\tilde{\Psi}_{k_1}(\hat{\theta}_{k_1})\}_{k_1=1}^{K_1} \in \mathbb{R}^{pK_1}$  and a final integrated estimator

$$\hat{\theta}_r = \mathbf{J}_0^{-1}(\hat{\theta}_{k_1}) \mathbf{S}_0(\hat{\theta}_{k_1}) \mathbf{V}_0^{-1}(\hat{\theta}_{k_1}) \left[ \{ \mathbf{S}_0^\top(\hat{\theta}_{k_1}) \}_j \hat{\theta}_j \right]_{j=1}^{K_1},\tag{6}$$

where  $\mathbf{V}_0(\hat{\theta}_{k_1}) = \sum_{i=1}^N \{\psi_{i,0}(\hat{\theta}_{k_1})\}^{\otimes 2}$ ,  $\mathbf{S}_0(\hat{\theta}_{k_1}) = -\{\nabla_\theta \Psi_0(\theta)|_{\theta=\hat{\theta}_{k_1}}\}$  and

$$\mathbf{J}_0(\hat{\theta}_{k_1}) = \mathbf{S}_0(\hat{\theta}_{k_1}) \mathbf{V}_0^{-1}(\hat{\theta}_{k_1}) \mathbf{S}_0^\top(\hat{\theta}_{k_1}) \in \mathbb{R}^{p \times p},\tag{7}$$

can be computed following the recursive procedure. Next, we give a toy illustration of the procedure. Consider a  $10 \times 10$  grid of spatial locations  $\mathcal{A}_0 = \{(s_i, s_j)\}_{i,j=1}^{10}$  partitioned first into  $K_1 = 2$  regions  $\{\mathcal{A}_1, \mathcal{A}_2\}$  that are again partitioned into  $K_2 = 2$  regions  $\{\mathcal{A}_{11}, \mathcal{A}_{12}, \mathcal{A}_{21}, \mathcal{A}_{22}\}$ , illustrated in Figure 2. We compute  $\hat{\theta}_r$  as follows:



1. For  $m = 2$ , compute the kernel score functions  $\psi_{i,k_1k_2}(\boldsymbol{\theta})$ ,  $i = 1, \dots, N$ , to obtain MLEs  $\hat{\boldsymbol{\theta}}_{k_1k_2}$ ,  $k_1 = 1, 2$ ,  $k_2 = 1, 2$ .
2. For  $m = 1$ , define  $\psi_{i,k_1}(\hat{\boldsymbol{\theta}}_{k_1k_2}) = \{\psi_{i,k_11}^\top(\hat{\boldsymbol{\theta}}_{k_11}), \psi_{i,k_12}^\top(\hat{\boldsymbol{\theta}}_{k_12})\}^\top$ ,  $i = 1, \dots, N$ , so that we can compute  $\mathbf{V}_{k_1}(\hat{\boldsymbol{\theta}}_{k_1k_2}) = \sum_{i=1}^N \{\psi_{i,k_1}(\hat{\boldsymbol{\theta}}_{k_1k_2})\}^{\otimes 2}$ . This allows us to estimate the sensitivity with  $\mathbf{S}_{k_1}(\hat{\boldsymbol{\theta}}_{k_1k_2})$  and obtain  $\hat{\boldsymbol{\theta}}_{k_1}$  in (4) for  $k_1 = 1, 2$ .
3. For  $m = 0$ , recursively compute  $\mathbf{V}_0(\hat{\boldsymbol{\theta}}_{k_1}) = \sum_{i=1}^N [\{\tilde{\psi}_{i,k_1}(\hat{\boldsymbol{\theta}}_{k_1})\}_{k_1=1}^2]^{\otimes 2}$ ,  $\mathbf{S}_0(\hat{\boldsymbol{\theta}}_{k_1})$ ,  $\mathbf{J}_0(\hat{\boldsymbol{\theta}}_{k_1})$ :
  - (a) Compute the kernel score functions  $\psi_{i,k_1k_2}(\hat{\boldsymbol{\theta}}_{k_1})$ ,  $i = 1, \dots, N$ ,  $k_1 = 1, 2$ ,  $k_2 = 1, 2$ .
  - (b) Define  $\psi_{i,k_1}(\hat{\boldsymbol{\theta}}_{k_1}) = \{\psi_{i,k_11}^\top(\hat{\boldsymbol{\theta}}_{k_1}), \psi_{i,k_12}^\top(\hat{\boldsymbol{\theta}}_{k_1})\}^\top$  so that we can compute  $\mathbf{V}_{k_1}(\hat{\boldsymbol{\theta}}_{k_1}) = \sum_{i=1}^N \{\psi_{i,k_1}(\hat{\boldsymbol{\theta}}_{k_1})\}^{\otimes 2}$ , allowing us to estimate the sensitivity with  $\mathbf{S}_{k_1}(\hat{\boldsymbol{\theta}}_{k_1})$ ,  $k_1 = 1, 2$ .
  - (c) Compute  $\tilde{\psi}_{i,k_1}(\hat{\boldsymbol{\theta}}_{k_1}) = \mathbf{S}_{k_1}(\hat{\boldsymbol{\theta}}_{k_1})\mathbf{V}_{k_1}^{-1}(\hat{\boldsymbol{\theta}}_{k_1})\psi_{i,k_1}(\hat{\boldsymbol{\theta}}_{k_1})$ ,  $k_1 = 1, 2$ .

Then compute  $\mathbf{V}_0(\hat{\boldsymbol{\theta}}_{k_1})$ ,  $\mathbf{S}_0(\hat{\boldsymbol{\theta}}_{k_1})$  and  $\mathbf{J}_0(\hat{\boldsymbol{\theta}}_{k_1})$  to obtain  $\hat{\boldsymbol{\theta}}_r$ .

One evaluation at resolution  $M$  has computation and memory complexities of  $O\{N(pS_{k_1\dots k_M})^3\}$  and  $O\{N(pS_{k_1\dots k_M})^2\}$  respectively. This evaluation is repeated  $M$  times across the recursive integration procedure. The recursive loop inverts each  $(pK_m) \times (pK_m)$  covariance matrix  $O(M)$  times, adding computation and memory complexities  $O\{M(pK_m)^3\}$  and  $O\{M(pK_m)^2\}$  respectively. At each resolution  $m$ , inversions and the computation of the  $K_m$  estimators  $\hat{\boldsymbol{\theta}}_{k_1\dots k_m}$  can be done in parallel across  $K_m$  computing nodes to further reduce computational costs. This yields computation and memory complexities, respectively, of

$$O\left[\sum_{m=1}^M \left\{N(pS_{k_1\dots k_M})^3 + \max_{k_m=1,\dots,K_m} NM(pk_m)^3\right\}\right] = O\left\{NM(pS_{k_1\dots k_M})^3 + \max_{\substack{k_m=1,\dots,K_m \\ m=1,\dots,M}} NM^2(pk_m)^3\right\}$$

$$O\left[\sum_{m=1}^M \left\{N(pS_{k_1\dots k_M})^2 + \max_{k_m=1,\dots,K_m} NM(pk_m)^2\right\}\right] = O\left\{NM(pS_{k_1\dots k_M})^2 + \max_{\substack{k_m=1,\dots,K_m \\ m=1,\dots,M}} NM^2(pk_m)^2\right\}.$$

Finally, the computation of  $\hat{\boldsymbol{\theta}}_{k_1\dots k_m}$  requires no iterative minimization of an objective function, substantially reducing computational costs. It bears emphasizing that the procedure can be fully run on a distributed system, meaning that at no point do the data need to be loaded on a central server or the full  $S \times S$  covariance matrix stored.

### 3 Multi-Resolution Estimating Function Theory

Let  $\Theta$  the parameter space of  $\boldsymbol{\theta}$ , and denote by  $\boldsymbol{\theta}_0$  the true value of  $\boldsymbol{\theta}$ , defined formally by assumption (A1) in Appendix A. In this section, we study the asymptotic properties of  $\hat{\boldsymbol{\theta}}_r$  by formalizing a multi-resolution estimating function theory. To do this, first define population versions of the estimating functions, their variability and their sensitivity: for  $k_m = 1, \dots, K_m$ , let

$$\phi_{i,k_1\dots k_m}(\boldsymbol{\theta}) = \psi_{i,k_1\dots k_m}(\boldsymbol{\theta}), \quad m = M, M-1,$$

$$\begin{aligned}\tilde{\phi}_{i,k_1\dots k_m}(\boldsymbol{\theta}) &= \mathbf{s}_{k_1\dots k_m}(\boldsymbol{\theta})\mathbf{v}_{k_1\dots k_m}^{-1}(\boldsymbol{\theta})\phi_{i,k_1\dots k_m}(\boldsymbol{\theta}), \quad m = M-1, \dots, 1 \\ \phi_{i,k_1\dots k_m}(\boldsymbol{\theta}) &= \{\tilde{\phi}_{i,k_1\dots k_{m+1}}(\boldsymbol{\theta})\}_{k_{m+1}=1}^{K_{m+1}}, \quad m = M-2, \dots, 1,\end{aligned}$$

where, for  $m = 1, \dots, M$ ,  $\mathbf{v}_{k_1\dots k_m}(\boldsymbol{\theta}) = \mathbb{V}_{\boldsymbol{\theta}_0} \{\phi_{i,k_1\dots k_m}(\boldsymbol{\theta})\}$ ,  $\mathbf{s}_{k_1\dots k_m}^\top(\boldsymbol{\theta}) = -\mathbb{E}_{\boldsymbol{\theta}_0} \{\nabla_{\boldsymbol{\theta}} \phi_{i,k_1\dots k_m}(\boldsymbol{\theta})\}$  and  $\mathbf{j}_{k_1\dots k_m}(\boldsymbol{\theta}) = \mathbf{s}_{k_1\dots k_m}(\boldsymbol{\theta})\mathbf{v}_{k_1\dots k_m}^{-1}(\boldsymbol{\theta})\mathbf{s}_{k_1\dots k_m}^\top(\boldsymbol{\theta})$  are the variability, sensitivity and Godambe information (Godambe, 1991) matrices, respectively, in  $\mathcal{A}_{k_1\dots k_m}$ . Let  $\phi_{i,0}(\boldsymbol{\theta}) = \{\tilde{\phi}_{i,k_1}(\boldsymbol{\theta})\}_{k_1=1}^{K_1}$ , and define  $\mathbf{v}_0(\boldsymbol{\theta}) = \mathbb{V}_{\boldsymbol{\theta}_0} \{\phi_{i,0}(\boldsymbol{\theta})\}$ ,  $\mathbf{s}_0^\top(\boldsymbol{\theta}) = -\mathbb{E}_{\boldsymbol{\theta}_0} \{\nabla_{\boldsymbol{\theta}} \phi_{i,0}(\boldsymbol{\theta})\}$  and  $\mathbf{j}_0(\boldsymbol{\theta}) = \mathbf{s}_0(\boldsymbol{\theta})\mathbf{v}_0^{-1}(\boldsymbol{\theta})\mathbf{s}_0^\top(\boldsymbol{\theta})$ . We assume throughout that  $\mathbf{v}_{k_1\dots k_m}(\boldsymbol{\theta}_0)$ , and  $\mathbf{v}_0(\boldsymbol{\theta}_0)$  are positive definite.

Under appropriate assumptions on the score functions  $\boldsymbol{\Psi}_{k_1\dots k_M}(\boldsymbol{\theta})$ , namely unbiasedness, uniqueness of the root and additivity, the  $K_M$  estimators  $\hat{\boldsymbol{\theta}}_{k_1\dots k_M}$  from the  $M$ th resolution are consistent for  $\boldsymbol{\theta}_0$  and semi-parametrically efficient within each  $\mathcal{A}_{k_1\dots k_M}$ ,  $k_M = 1, \dots, K_M$ . Moreover, under appropriate conditions,  $\hat{\boldsymbol{\theta}}_{k_1\dots k_{M-1}}$  is consistent and Hansen optimal by Hector and Song (2021). Finally, at each resolution, an optimal estimator is derived from the optimal GMM function (Hansen, 1982) and from optimal estimating function theory (Heyde, 1997). This results in a highly efficient integrated estimator  $\hat{\boldsymbol{\theta}}_r$  in (6) that fully uses the dependence within and between each resolution. This result is shown formally in Theorem 1.

**Theorem 1.** *Under assumptions (A1) as  $N \rightarrow \infty$ ,  $\hat{\boldsymbol{\theta}}_r$  in (6) is consistent and  $\sqrt{N}(\hat{\boldsymbol{\theta}}_r - \boldsymbol{\theta}_0) \xrightarrow{d} \mathcal{N}\{\mathbf{0}, \mathbf{j}_0^{-1}(\boldsymbol{\theta}_0)\}$ .*

The proof proceeds by induction after establishing consistency and asymptotic normality of the integrated estimators at resolution  $M-1$ . The key technique is a recursive Taylor expansion at each resolution to establish the appropriate convergence rate of the estimating function. Large sample confidence intervals for  $\boldsymbol{\theta}_0$  can be constructed by combining the asymptotic normality from Theorem 1 and the following Corollary.

**Corollary 1.** *Under assumptions (A1) as  $N \rightarrow \infty$ ,  $\mathbf{J}_0^{-1}(\hat{\boldsymbol{\theta}}_r)$  in (7) is a consistent estimator of the asymptotic covariance of  $\hat{\boldsymbol{\theta}}_r$  in (6).*

The proof follows from the proof of Theorem 1 and is omitted.

## 4 Sequential Model Integration Framework

The most time consuming step in the recursive integration procedure requires a recursive update of the weights each time a new estimator of  $\boldsymbol{\theta}$  is computed at resolution  $m = M-2, \dots, 0$ , as illustrated on the left of Figure 3. This is because the weight matrices  $\mathbf{V}_{k_1\dots k_m}(\hat{\boldsymbol{\theta}}_{k_1\dots k_{m+1}})$  and  $\mathbf{S}_{k_1\dots k_m}(\hat{\boldsymbol{\theta}}_{k_1\dots k_{m+1}})$  are evaluated at  $\hat{\boldsymbol{\theta}}_{k_1\dots k_{m+1}}$ . This recursive integration procedure has time complexity which depends on  $M^2$ , which may be undesirably slow. We propose an alternate sequential integration scheme that evaluates the weight at the estimator from the  $M$ th resolution,  $\hat{\boldsymbol{\theta}}_{k_1\dots k_M}$ , a consistent estimator for  $\boldsymbol{\theta}$ , illustrated on the right of Figure 3. The sequential integration procedure replaces the recursive evaluation of the weights with a sequential update by computing  $\mathbf{V}_{k_1\dots k_m}(\hat{\boldsymbol{\theta}}_{k_1\dots k_M})$  and  $\mathbf{S}_{k_1\dots k_m}(\hat{\boldsymbol{\theta}}_{k_1\dots k_M})$ . In this fashion, no recursive update of the weights is required. We denote by  $\hat{\boldsymbol{\theta}}_s$  the sequential integrated estimator obtained by evaluating weights using  $\mathbf{V}_{k_1\dots k_m}(\hat{\boldsymbol{\theta}}_{k_1\dots k_M})$  and  $\mathbf{S}_{k_1\dots k_m}(\hat{\boldsymbol{\theta}}_{k_1\dots k_M})$ . A full algorithm is provided in the supplement.

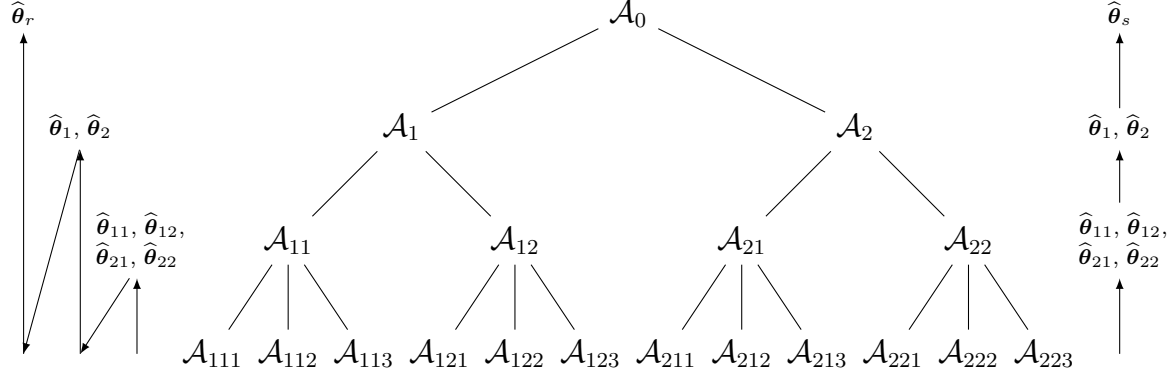


Figure 3: Example partition of  $\mathcal{A}_0$  with  $M = 3$  resolutions. Schematic propagation steps for computation of  $\hat{\theta}_{k_1 \dots k_m}$  for recursive (left) and sequential (right) integration schemes.

By a similar analysis to Section 2.3.3, the computation and memory complexities of computing  $\hat{\theta}_s$  are

$$O\left\{N(pS_{k_1 \dots k_M})^3 + \max_{\substack{k_m=1, \dots, K_m \\ m=1, \dots, M}} NM(pk_m)^3\right\}, \quad O\left\{N(pS_{k_1 \dots k_M})^2 + \max_{\substack{k_m=1, \dots, K_m \\ m=1, \dots, M}} NM(pk_m)^2\right\},$$

respectively. A consequence of the proof of Theorem 1 is that  $\hat{\theta}_s$  and  $\hat{\theta}_r$  are asymptotically equivalent. While  $\hat{\theta}_s$  may be computationally more advantageous, it requires that the MLEs from resolution  $M$  be close to  $\theta_0$ , and may not perform as well as  $\hat{\theta}_r$  in finite samples.

## 5 Simulations

We investigate the finite sample performance of the proposed recursive and sequential multi-resolution recursive integrated (MRRI) estimators  $\hat{\theta}_r$  and  $\hat{\theta}_s$ . Throughout,  $\mathcal{S}$  consists of a square grid of evenly spaced locations. The Gaussian outcomes  $\{y_i(\mathcal{S})\}_{i=1}^N$  are independently simulated with means  $\{\mathbf{X}_i^\top(\mathcal{S})\boldsymbol{\beta}\}_{i=1}^N$  and Matérn spatial covariance function  $C_\alpha(\cdot, \cdot; \boldsymbol{\gamma})$ , with  $\boldsymbol{\beta}$ ,  $\boldsymbol{\gamma}$  and nugget variance  $\sigma^2$  specified below. Two observations  $y_i(\mathbf{s}_1)$  and  $y_i(\mathbf{s}_2)$ , separated by a Euclidean distance of  $t$ , have covariance  $\tau^2 2^{1-\nu} / \Gamma(\nu) (\sqrt{2\nu}\phi^2 t) K_\nu(\sqrt{2\nu}\phi^2 d)$ , where  $\Gamma$  is the Gamma function and  $K_\nu$  is the modified Bessel function of the second kind,  $\nu$  is treated as fixed and  $\boldsymbol{\gamma} = (\tau^2, \phi^2)$ . Unless otherwise specified, all simulations are on a Linux cluster using R linked to Intel's MKL libraries with analyses at resolution  $M$  performed in parallel across  $\tilde{K} = \prod_{m=1}^M K_m$  CPUs with 1GB of RAM each. Standard errors and confidence intervals are calculated using the asymptotic normality results in Theorem 1 and Corollary 1.

In the first set of simulations, we consider a  $S = 400$ -dimensional square spatial domain  $\mathcal{D} = [1, 20]^2 = \{\mathbf{s}_j\}_{j=1}^{400}$ ,  $\mathbf{s}_j \in \mathbb{R}^2$ , with  $N = 10000$ . The covariates  $\mathbf{X}_i(\mathbf{s}_j) = \mathbf{X}_i$  consist of an intercept and two non-spatially varying continuous variables generated from a Gaussian distribution with mean 0 and variance 4. The true value of the regression coefficient is  $\boldsymbol{\beta} = (0.3, 0.6, 0.8)$ . The true nugget variance is  $\sigma^2 = 1.6$  and the Matérn spatial covariance function has true parameters  $\tau^2 = 3$  and  $\phi^2 = 0.5$  with  $\nu = \infty$ , reducing to a Gaussian covariance function. To improve numeric performance, we estimate  $\boldsymbol{\theta} = \{\boldsymbol{\beta}, \log(\sigma^2), \log(\tau^2), \log(\phi^2)\}$

using  $\hat{\theta}_r$  and  $\hat{\theta}_s$ . We consider three recursive partitions of  $S$  with  $M = 3$ : in Setting I,  $K_1 = K_2 = 2, K_3 = 4$ ; in Setting II,  $K_1 = K_3 = 2, K_2 = 4$ ; in Setting III,  $K_1 = 4, K_2 = K_3 = 2$ . Division of the spatial domain is based on nearest neighbours as illustrated in Figure 2. We also estimate  $\theta$  using two comparative approaches. Specifically, we compare to the partitioning approach (Part.) in Heaton et al. (2019) that evaluates the sum of the  $\tilde{K}$  log-likelihoods at a grid of values of  $\tau^2, \phi^2$ , estimates  $\tau^2, \phi^2$  using the values that return the highest log-likelihood, then estimates  $\beta$  and  $\sigma^2$  using the least squares estimator and a sample variance respectively; the implementation is modified directly from the code available in Heaton et al. (2019). Asymptotic standard errors are estimated as the diagonal square root of the inverse variance of the score function. We also compare to the nearest neighbour Gaussian process (NNGP) (Finley et al., 2019) using the 25 nearest neighbours; we implement this ourselves using sparse matrices in Rcpp and parallelize over  $\tilde{K}$  CPUs to make a fair comparison. Figure 4 plots the root mean squared error (RMSE), empirical standard error (ESE) and asymptotic standard error (ASE) averaged across 500 simulations for each parameter.

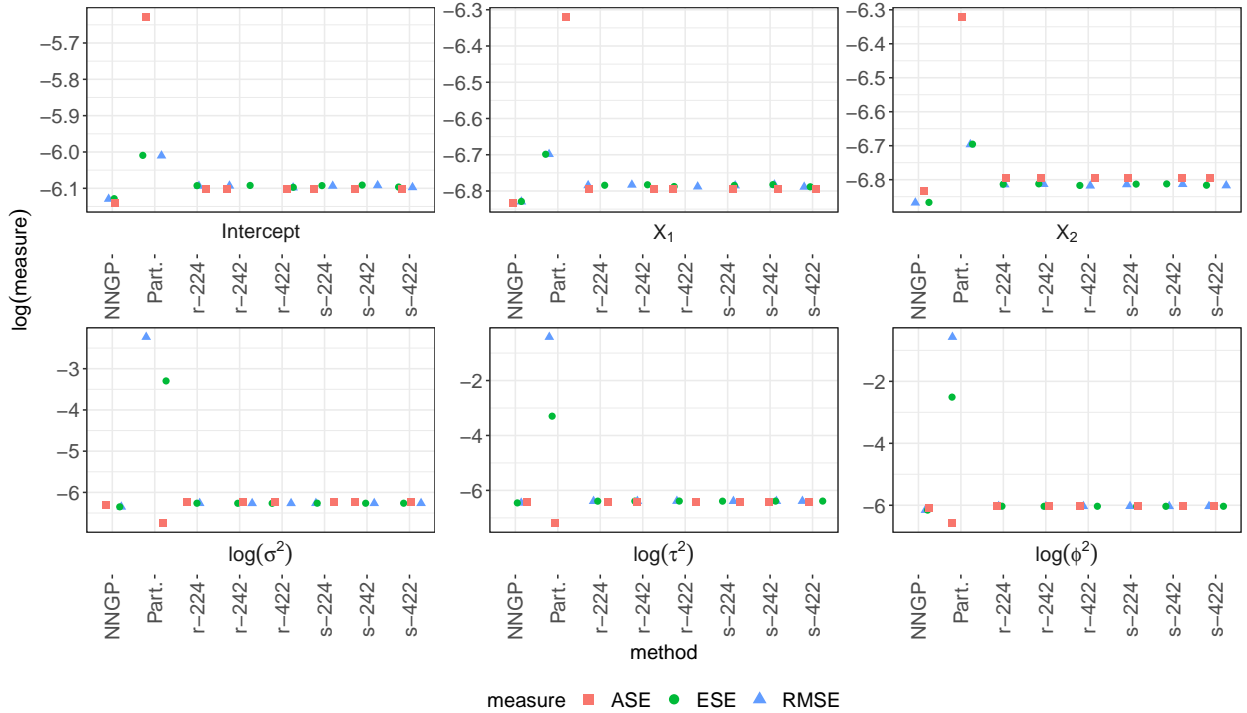


Figure 4: RMSE, ESE and ASE for estimates of each parameter using NNGP, Part.,  $\hat{\theta}_r$  and  $\hat{\theta}_s$  in Settings I, II and III (r-224, r-242, r-422, s-224, s-242, s-422 respectively) for the first set of simulations.

The near equality of RMSE and ESE in Figure 4 for our MRRI estimators  $\hat{\theta}_r$  and  $\hat{\theta}_s$  illustrates the near unbiasedness of our approach in large samples. Further, the near equality of ESE and ASE justifies the use of the asymptotic variance formula in Theorem 1 and Corollary 1 in large samples. Finally, negligible variation is observed across Settings I, II and III, illustrating the robustness of our approach to the chosen recursive or sequential

integration scheme. The statistical inference properties of NNGP are similarly favourable, with the NNGP appearing slightly more efficient. Finally, the partitioning approach yields estimators of  $\beta$  that are near unbiased in large samples, whereas the estimators of the covariance parameters show substantial bias. Further, standard errors of the estimators are vastly overestimated for  $\beta$  and underestimated for the covariance parameters, which is problematic for statistical inference. This is further illustrated in Table 1, which reports the 95% confidence interval coverage (CP) for all estimators averaged across 500 simulations. Whereas CP reaches nominal levels across parameters for MRRI and NNGP, regression and covariance parameters are respectively overcovered and undercovered using the partitioning approach.

Table 1: 95% confidence interval coverage (CP) in percentage for first set of simulations:  $S = 400$ ,  $\theta = \{0.3, 0.6, 0.8, \log(1.6), \log(3), \log(0.5)\}$ .

| Method           | $K_1, K_2, K_3$ | Intercept | $X_1$ | $X_2$ | $\log(\sigma^2)$ | $\log(\tau^2)$ | $\log(\phi^2)$ |
|------------------|-----------------|-----------|-------|-------|------------------|----------------|----------------|
| $\hat{\theta}_r$ | 2, 2, 4         | 94.2      | 95.6  | 94.4  | 94.6             | 96.2           | 93.4           |
|                  | 2, 4, 2         | 94.8      | 95.6  | 94.4  | 94.8             | 96.0           | 93.2           |
|                  | 4, 2, 2         | 94.4      | 95.2  | 94.8  | 94.6             | 96.0           | 93.4           |
| $\hat{\theta}_s$ | 2, 2, 4         | 94.2      | 95.8  | 94.4  | 94.8             | 96.0           | 93.4           |
|                  | 2, 4, 2         | 94.6      | 95.6  | 94.4  | 95.0             | 96.0           | 93.4           |
|                  | 4, 2, 2         | 94.4      | 95.2  | 94.6  | 95.0             | 95.8           | 93.4           |
| Part.            |                 | 99.6      | 99.6  | 100   | 0                | 0              | 0              |
| NNGP             |                 | 94.6      | 95.2  | 95.4  | 95.8             | 96.4           | 95.8           |

Computing times in seconds are reported in Table 2. We see evidence of the small computational cost of recursively updating weights with  $\hat{\theta}_r$  over using the weights computed at the  $M$ th layer with  $\hat{\theta}_s$ . In comparison, the partitioning and NNGP approaches are 212 and 467 times slower, respectively, than our sequential integrated estimator  $\hat{\theta}_s$  with  $K_1 = 4, K_2 = K_3 = 2$ .

Table 2: Mean elapsed time (Monte Carlo standard deviation) in seconds of  $\hat{\theta}_r$ ,  $\hat{\theta}_s$ , NNGP and Part. across 500 simulation for the first set of simulations:  $S = 400$ ,  $\theta = \{0.3, 0.6, 0.8, \log(1.6), \log(3), \log(0.5)\}$ .

| Method           | $K_1, K_2, K_3 = 2, 2, 4$ | $K_1, K_2, K_3 = 2, 4, 2$ | $K_1, K_2, K_3 = 4, 2, 2$ | 16 CPUs   |
|------------------|---------------------------|---------------------------|---------------------------|-----------|
| $\hat{\theta}_r$ | 0.80 (0.092)              | 0.66 (0.060)              | 0.66 (0.060)              |           |
| $\hat{\theta}_s$ | 0.72 (0.084)              | 0.60 (0.064)              | 0.60 (0.064)              |           |
| NNGP             |                           |                           |                           | 280 (140) |
| Part.            |                           |                           |                           | 127 (11)  |

In the second set of simulations, we consider a  $S = 25600$ -dimensional square spatial domain  $\mathcal{D} = [1, 160]^2 = \{\mathbf{s}_j\}_{j=1}^{25600}$ ,  $\mathbf{s}_j \in \mathbb{R}^2$ , with  $N = 5000$  in Setting I and  $N = 2000$  in Setting II. The covariates are generated as in the first set of simulations. The true value of  $\theta$  is the same as the first set of simulations, and we estimate  $\theta = \{\beta, \log(\sigma^2), \log(\tau^2), \log(\phi^2)\}$  using  $\hat{\theta}_r$  and  $\hat{\theta}_s$  by recursively partitioning  $S$  with  $M = 4$ ,  $K_1 = K_2 = K_3 = K_4 = 4$ . Division of the spatial domain is based on nearest neighbours as illustrated in Figure 2. Analyses

are parallelized across 16 CPUs with 2GB of RAM each. Given the poor performance of the partitioning approach in the first set of simulations, we only attempted to compare to the NNGP using the 100 nearest neighbours parallelized over 16 CPUs. Unfortunately, not one of the 500 simulations finished before the computation timed out at 24 hours. Table 3 reports the RMSE, ESE, ASE, mean bias (BIAS) and CP of our MRRI estimators averaged across 500 simulations for each parameter.

Table 3: Simulation metrics of  $\hat{\theta}_r$  and  $\hat{\theta}_s$  across 500 simulations for the second set of simulations:  $S = 25600$ ,  $\theta = \{0.3, 0.6, 0.8, \log(1.6), \log(3), \log(0.5)\}$ .

| (a) Simulation metrics in Setting I.  |                       |                    |                   |                   |                    |        |
|---------------------------------------|-----------------------|--------------------|-------------------|-------------------|--------------------|--------|
| Estimator                             | Parameter             | RMSE $\times 10^4$ | ESE $\times 10^4$ | ASE $\times 10^4$ | BIAS $\times 10^5$ | CP (%) |
| $\hat{\theta}_r$                      | Intercept             | 4.2                | 4.2               | 4.1               | -2.7               | 96     |
|                                       | $\mathbf{X}_1$ effect | 2.0                | 2.0               | 2.1               | 0.021              | 96     |
|                                       | $\mathbf{X}_2$ effect | 2.1                | 2.1               | 2.1               | 0.42               | 94     |
|                                       | $\log(\sigma^2)$      | 3.2                | 3.1               | 3.1               | -3.3               | 96     |
|                                       | $\log(\tau^2)$        | 2.7                | 2.7               | 2.8               | -1.7               | 96     |
|                                       | $\log(\phi^2)$        | 4.1                | 4.0               | 3.7               | 8.7                | 93     |
| $\hat{\theta}_s$                      | Intercept             | 4.2                | 4.2               | 4.1               | -2.7               | 96     |
|                                       | $\mathbf{X}_1$ effect | 2.0                | 2.0               | 2.0               | 0.073              | 96     |
|                                       | $\mathbf{X}_2$ effect | 2.1                | 2.1               | 2.0               | 0.42               | 94     |
|                                       | $\log(\sigma^2)$      | 3.2                | 3.1               | 3.1               | -3.5               | 95     |
|                                       | $\log(\tau^2)$        | 2.7                | 2.7               | 2.8               | -2.2               | 96     |
|                                       | $\log(\phi^2)$        | 4.1                | 4.0               | 3.7               | 9.4                | 93     |
| (b) Simulation metrics in Setting II. |                       |                    |                   |                   |                    |        |
| Estimator                             | Parameter             | RMSE $\times 10^4$ | ESE $\times 10^4$ | ASE $\times 10^4$ | BIAS $\times 10^4$ | CP (%) |
| $\hat{\theta}_r$                      | Intercept             | 6.5                | 6.5               | 6.5               | -0.69              | 95     |
|                                       | $\mathbf{X}_1$ effect | 3.4                | 3.4               | 3.2               | -0.073             | 93     |
|                                       | $\mathbf{X}_2$ effect | 3.4                | 3.4               | 3.2               | 0.044              | 94     |
|                                       | $\log(\sigma^2)$      | 5.1                | 5.1               | 4.8               | -0.40              | 92     |
|                                       | $\log(\tau^2)$        | 4.5                | 4.5               | 4.4               | -0.28              | 94     |
|                                       | $\log(\phi^2)$        | 6.4                | 6.3               | 5.9               | 1.3                | 93     |
| $\hat{\theta}_s$                      | Intercept             | 6.5                | 6.5               | 6.4               | -0.72              | 94     |
|                                       | $\mathbf{X}_1$ effect | 3.4                | 3.4               | 3.2               | -0.065             | 93     |
|                                       | $\mathbf{X}_2$ effect | 3.4                | 3.4               | 3.2               | 0.057              | 94     |
|                                       | $\log(\sigma^2)$      | 5.1                | 5.1               | 4.8               | -0.43              | 92     |
|                                       | $\log(\tau^2)$        | 4.5                | 4.5               | 4.4               | -0.39              | 94     |
|                                       | $\log(\phi^2)$        | 6.4                | 6.3               | 5.9               | 1.4                | 93     |

Again, simulation metrics in Table 3 support the use of Theorem 1 and Corollary 1 in finite samples: the RMSE, ESE and ASE are approximately equal, and the BIAS is negligible. We observe appropriate confidence interval coverage (CP), with a slight undercoverage in Setting II with a smaller sample size. Further, the recursive and sequential integrated estimators appear equivalent in these large sample size settings. We also confirm that the desirable statistical performance observed in the first set of simulations remains as we increase the number of resolutions,  $M$ . Finally, computing times in seconds are reported in Table 4.

Again, we see the substantial computational superiority of the MRRI approach over the NNGP, which could not be run.

Table 4: Mean elapsed time (Monte Carlo standard deviation) in seconds of  $\hat{\theta}_r$  and  $\hat{\theta}_s$  across 500 simulations for the second set of simulations in Settings I and II:  $S = 25600$ ,  $\theta = \{0.3, 0.6, 0.8, \log(1.6), \log(3), \log(0.5)\}$ .

| Method           | Setting I | Setting II |
|------------------|-----------|------------|
| $\hat{\theta}_r$ | 390 (170) | 240 (110)  |
| $\hat{\theta}_s$ | 380 (140) | 230 (89)   |

## 6 Estimation of Brain Functional Connectivity

We return to the motivating neuroimaging application described in Section 1. Out of 1112 ABIDE participants,  $N = 774$  passed quality control: 379 with ASD, 647 males (335 with ASD) and 127 females (44 with ASD), with mean age 15 years (standard deviation 6 years). The left and right precentral gyri form the primary motor cortex and are responsible for executing voluntary movements (Bookheimer, 2013). They are two of the largest regions of interest (ROI) in the Harvard-Oxford atlas (FMRIB Software Library, 2018) with 1786 and 1888 voxels respectively. Many individuals with ASD have motor deficits (Jansiewicz et al., 2006). Atypical connectivity between the left and right precentral gyri may indicate that these motor deficits are related to how these two brain regions coordinate movement. The pre-processing pipeline of rfMRI data has already been described by Craddock et al. (2013). Notably, participant-specific data have been registered into a common template space such that voxel locations are comparable between participants in the study.

Denote the rfMRI outcomes in the left and right precentral gyri by  $\{z_i(\mathbf{v}_{1j_1}, t)\}_{j_1=1}^{1786}$  and  $\{z_i(\mathbf{v}_{2j_2}, t)\}_{j_2=1}^{1888}$ , respectively, for voxel locations  $\mathbf{v}_{1j_1}, \mathbf{v}_{2j_2} \in \mathbb{R}^3$ ,  $t = 1, \dots, T_i$ . We study the correlation between voxels in the two ROI. Using the time series for participant  $i$  at each pair of voxel locations  $(\mathbf{v}_{1j_1}, \mathbf{v}_{2j_2})$ , we estimate the  $S = 1786 \times 1888 = 3371968$  correlations  $y_i(\mathbf{s}_j) = \text{cor}\{z_i(\mathbf{v}_{1j_1}, t), z_i(\mathbf{v}_{2j_2}, t)\}$  between voxels in the left and right precentral gyri. Letting  $\mathcal{S} = \{\mathbf{s}_j\}_{j=1}^{3371968}$ , we thus observe  $y_i(\mathcal{S})$  at  $S = 3371968$  voxel-pair locations  $\mathbf{s}_j = (\mathbf{v}_{1j_1}, \mathbf{v}_{2j_2})$ ,  $j = 1888(j_1 - 1) + j_2$ ,  $i = 1, \dots, 774$ . Due to the length of the time series  $T_i$ ,  $y_i(\mathbf{s}_j)$  is approximately Gaussian distributed. In addition, we investigated the normality of the correlations with Q-Q plots (including in the supplement) and deemed that the correlations  $y_i(\mathbf{s}_j)$  appeared approximately Gaussian and that a Fisher  $z$ -transformation was not necessary. Correlations  $y_i(\mathbf{s}_j)$  for participant  $i$  that fall within  $\mathcal{S}$  but that are undefined because  $z_i(\mathbf{v}_{1j_1}, t)$  and/or  $z_i(\mathbf{v}_{2j_2}, t)$  are 0 for all  $t = 1, \dots, T_i$  are treated as missing completely at random; this occurs because the Harvard-Oxford atlas does not provide a perfect template for all participants due to coregistration errors when transforming participant level data into a common template.

Let  $\{\mathbf{X}_i\}_{i=1}^N$  be corresponding  $N = 774$  observations of  $q = 5$  covariates for participant  $i$ : an intercept, ASD status (1 for ASD, 0 for neurotypical), age, sex (1 for male, 0 for female) and the age by ASD status interaction. We model  $\mu(\mathbf{X}_i, \boldsymbol{\beta}) = \mathbf{X}_i^\top \boldsymbol{\beta}$ , where  $\mu(\mathbf{X}_i, \boldsymbol{\beta})$  is the mean correlation between voxels in the left and right precentral gyri. We model the spatial



covariance  $\mathbf{C}_\alpha(\mathbf{s}_i, \mathbf{s}_j; \tau^2, \phi^2)$  as the Gaussian correlation function  $\tau^2 \exp(-\phi^2 \|\mathbf{s}_i - \mathbf{s}_j\|_2^2)$ .

The size of the analytic dataset is 163GB: it cannot be loaded in R, let alone analyzed, in its entirety. A distributed estimation approach is the only possible approach. To partition the six-dimensional spatial domain, we first assign  $\{K_m\}_{m=1}^M$  as the  $M = 7$  smallest divisors of  $S = 3371968$ ; we then run the K-means algorithm to cluster voxel-pair locations into  $K_1 \dots K_M$  regions  $\mathcal{A}_{k_1 \dots k_M}$ ; finally, we group regions at resolution  $m + 1$  according to shortest distance at each resolution  $m$ . Given this parcellation, we partition  $\mathcal{S}$  into  $K_1 = 2$  regions  $\mathcal{A}_1, \mathcal{A}_2$  of size  $S_{k_1} = 1685984$ , that are each again partitioned into  $K_2 = 2$  regions  $\{\mathcal{A}_{k_1 1}, \mathcal{A}_{k_1 2}\}_{k_1=1}^{K_1}$  of size  $S_{k_1 k_2} = 842992$ , that are each again partitioned into  $K_3 = 2$  regions  $\{\mathcal{A}_{k_1 k_2 1}, \dots, \mathcal{A}_{k_1 k_2 4}\}_{k_1, k_2=1}^{K_1, K_2}$  of size  $S_{k_1 k_2 k_3} = 421496$ , and so on with  $K_4 = 2, K_5 = 2, K_6 = 47$ , until we partition each  $S_{k_1 \dots k_6}$  into  $K_7 = 19$  regions  $\{\mathcal{A}_{k_1 \dots k_6 1}, \dots, \mathcal{A}_{k_1 \dots k_6 19}\}_{k_1, \dots, k_6=1}^{K_1, \dots, K_6}$  of size  $S_{k_1 \dots k_7} \in [42, 204]$ . This partition is depicted in Figure 5.

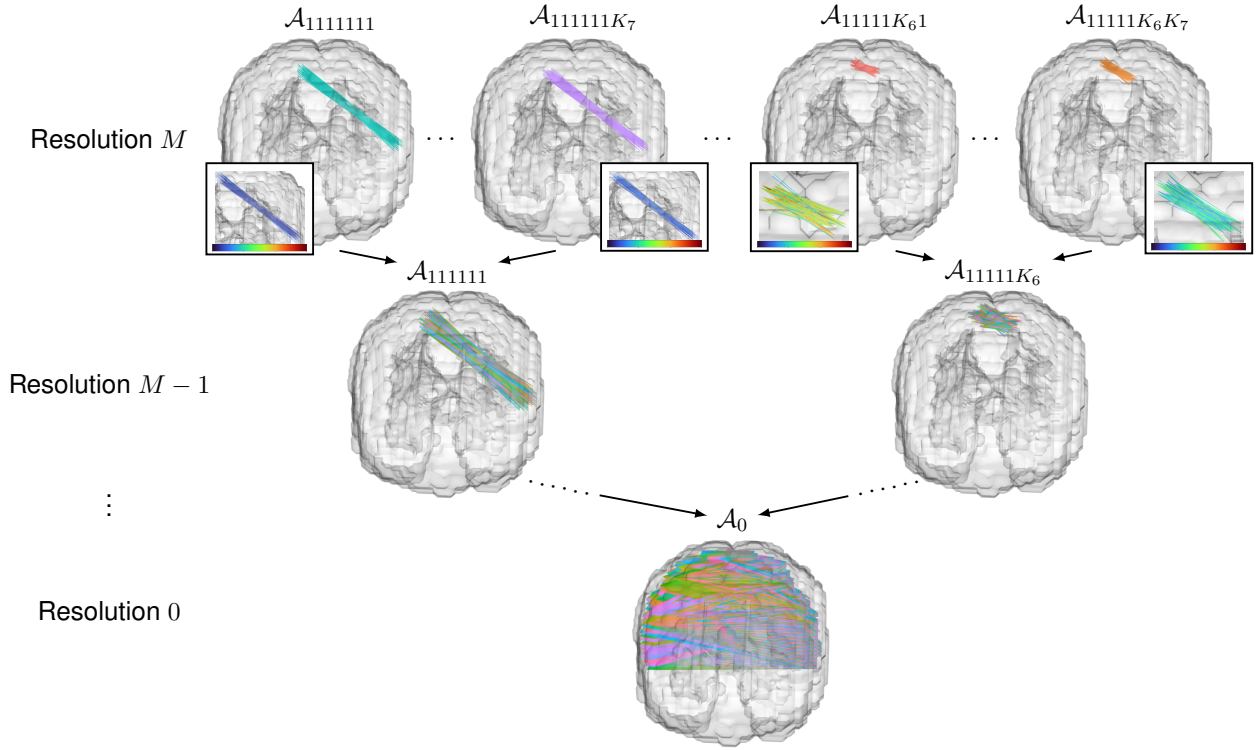


Figure 5: Recursive partition of the set of left and right precentral gyri voxel pairs with  $M = 7$ . Outcomes  $y_i(\mathbf{s}_j)$  are represented by lines between voxels: colors in thumbnails indicate the value of  $y_i(\mathbf{s})$  (i.e. correlation) ranging from 0 to 0.15, whereas colors in whole-brain images indicate the set to which the outcome belongs.

The estimated effects (s.d.) are  $-0.0534$  ( $6.73 \times 10^{-5}$ ),  $0.000196$  ( $3.9 \times 10^{-6}$ ),  $9.42 \times 10^{-5}$  ( $1.55 \times 10^{-7}$ ),  $0.00048$  ( $1.66 \times 10^{-6}$ ),  $-4.97 \times 10^{-5}$  ( $2.12 \times 10^{-7}$ ) for the intercept, ASD status, age, sex and age-ASD status interaction respectively. ASD status is significantly associated with increased functional connectivity between the left and right precentral gyri at level 0.05, adjusting for age and sex. Moreover, age is a significant modifier of the ASD effect. The estimates (s.d.) of the Gaussian covariance parameters  $\sigma^2, \tau^2, \phi^2$  on the log-scale are  $-8.3$  ( $9.84 \times 10^{-5}$ ),  $-3.26$  ( $0.000202$ ),  $-0.861$  ( $7.12 \times 10^{-5}$ ) respectively, giving a spatial covariance

$C_\alpha(\mathbf{s}_i, \mathbf{s}_j; \tau^2, \phi^2) = 0.038 \exp(-0.42 \|\mathbf{s}_i - \mathbf{s}_j\|_2^2)$  and an error variance  $\sigma^2 = 2.5 \times 10^{-4}$ . This suggests a strong positive correlation between voxel-pair correlations; ignoring this dependence would lead to a substantial loss of statistical power. Parallelized over 64 or 128 CPUs, this analysis of 3371968 outcomes takes 64 or 35 minutes respectively.

To illustrate the gain in statistical efficiency from our whole-brain modeling approach, we compare to the dominant approach in functional connectivity modeling. Functional connectivity between the left and right precentral gyri is estimated from the subject-specific correlation between the two rfMRI time series averaged across voxels in each ROI (Wang et al., 2010; He et al., 2009). The functional connectivity is regressed onto ASD status, age, sex and age-ASD status interaction. The estimated effects (s.d.) are 0.686 ( $2.68 \times 10^{-156}$ ),  $-0.0384$  (0.157), 0.00262 (0.0327),  $-0.0111$  (0.417),  $-4.82 \times 10^{-4}$  (0.771) for the intercept, ASD status, age, sex and age-ASD status interaction respectively. The standard deviations are orders of magnitude larger, and only the intercept is statistically significant at level 0.05. Our substantially more powerful approach to functional connectivity modeling uncovers is crucial to uncover new associations with ASD.

## 7 Discussion

The proposed recursive and sequential integration estimators depend on the choice of the recursive partition of  $\mathcal{S}$ . We have suggested that this partitioning be performed such that  $S_{k_1 \dots k_m}$  and  $K_m$ ,  $m = 1, \dots, M$  are relatively small compared to  $S_0$  and shown through simulations that this leads to desirable statistical and computational performance. Nonetheless, it is worth remarking that the GMM is known to underestimate the variance of estimators when  $K_m$  is moderately large relative to  $N$ ; see Hansen et al. (1996) and others in the special issue. Thus, special care should be taken to ensure  $K_m$  is relatively low-dimensional.

In this paper, we have assumed that  $\boldsymbol{\theta}$  does not vary spatially, and that it can be consistently estimated using subsets of the spatial domain  $\mathcal{S}$ . Future research should focus on the development of recursive and sequential integration rules for partially heterogeneous parameters  $\boldsymbol{\theta}$  following, for example, the work of Hector and Reich (2023) in spatially varying coefficient models. *A priori*, these extensions should follow from zero-padding the weight matrices in equations (4) and (6) and implementing a diligent accounting system to keep track of the heterogeneous and homogeneous model parameters, although a thorough empirical investigation needs to be performed to validate this extension.

## Acknowledgements

The authors are grateful to the participants of the ABIDE study, and the ABIDE study organizers and members who aggregated, preprocessed and shared the ABIDE data.

# A Appendices

## (A1) Basic Assumptions

- (i) The score functions  $\Psi_{k_1 \dots k_M}(\boldsymbol{\theta})$  are unbiased: for all  $\boldsymbol{\theta} \in \Theta$ ,  $\mathbb{E}_{\boldsymbol{\theta}} \Psi_{k_1 \dots k_M}(\boldsymbol{\theta}) = \mathbf{0}$ .
- (ii) The expectation  $\mathbb{E}_{\boldsymbol{\theta}_0} \Psi_{k_1 \dots k_M}(\boldsymbol{\theta})$  has a unique zero at  $\boldsymbol{\theta}_0$ .
- (iii) The score functions  $\Psi_{k_1 \dots k_M}(\boldsymbol{\theta})$  are continuously differentiable in a neighbourhood of  $\boldsymbol{\theta}_0$ .

# B Bibliography

- Alaerts, K., Woolley, D. G., Steyaert, J., Di Martino, A., Swinnen, S. P., and Wenderoth, N. (2014). Underconnectivity of the superior temporal sulcus predicts emotion recognition deficits in autism. *Social Cognitive and Affective Neuroscience*, 9(10):1589–1600.
- Appel, M. and Pebesma, E. (2020). Spatiotemporal multi-resolution approximations for analyzing global environment data. *Spatial Statistics*, 38:100465.
- Bai, Y., Song, P. X.-K., and Raghunathan, T. (2012). Joint composite estimating functions in spatiotemporal models. *Journal of the Royal Statistical Society, Series B*, 74(5):799–824.
- Banerjee, S., Carlin, B. P., and Gelfand, A. E. (2014). *Hierarchical modeling and analysis for spatial data*. Chapman & Hall.
- Banerjee, S., Gelfand, A. E., Finley, A. O., and Sang, H. (2008). Gaussian predictive process models for large spatial data sets. *Journal of the Royal Statistical Society, Series B*, 70(4):825–848.
- Bevilacqua, M., Gaetan, C., Mateu, J., and Porcu, E. (2012). Estimating space and space-time covariance functions for large data sets: a weighted composite likelihood approach. *Journal of the American Statistical Association*, 107(497):268–280.
- Bevilacqua, M., Mateu, J., Porcu, E., Zhang, H., and Zini, A. (2010). Weighted composite likelihood-based tests for space-time separability of covariance functions. *Statistics and Computing*, 20:283–293.
- Bookheimer, S. Y. (2013). *Precentral Gyrus*, pages 2334–2335. Springer New York, New York, NY.
- Bradley, J. R., Cressie, N. A., and Shi, T. (2016). A comparison of spatial predictors when datasets could be very large. *Statistics Surveys*, 10:100–131.
- Caragea, P. C. and Smith, R. L. (2007). Asymptotic properties of computationally efficient alternative estimators for a class of multivariate normal models. *Journal of Multivariate Analysis*, 98(7):1417–1440.
- Cessie, S. L. and van Houwelingen, J. (1994). Logistic regression for correlated binary data. *Journal of the Royal Statistical Society, Series C*, 43(1):95–108.

- Cox, D. R. and Reid, N. (2004). A note on pseudolikelihood constructed from marginal densities. *Biometrika*, 91(3):729–737.
- Craddock, C., Benhajali, Y., Chu, C., Chouinard, F., Evans, A., Jakab, A., Khundrakpam, B. S., Lewis, J. D., Li, Q., Milham, M., Yan, C., and Bellec, P. (2013). The Neuro Bureau Preprocessing Initiative: open sharing of preprocessed neuroimaging data and derivatives. In *Neuroinformatics*, Stockholm, Sweden.
- Cressie, N. A. (1993). *Statistics for spatial data*. Wiley, New York.
- Cressie, N. A. and Johannesson, G. (2008). Fixed rank kriging for very large spatial data sets. *Journal of the Royal Statistical Society, Series B*, 70(1):209–226.
- Cressie, N. A. and Wikle, C. K. (2015). *Statistics for spatio-temporal data*. Wiley.
- Curriero, F. C. and Lele, S. (1999). A composite likelihood approach to semivariogram estimation. *Journal of Agricultural, Biological and Environmental Statistics*, 4(1):9–28.
- Datta, A., Banerjee, S., Finley, A. O., and Gelfand, A. E. (2016a). Hierarchical nearest-neighbour Gaussian process models for large geostatistical datasets. *Journal of the American Statistical Association*, 111(514):800–812.
- Datta, A., Banerjee, S., Finley, A. O., Hamm, N. A., and Schaap, M. (2016b). Nonseparable dynamic nearest neighbour Gaussian process models for large spatio-temporal data with an application to particulate matter analysis. *The Annals of Applied Statistics*, 10(3):1286–1316.
- Di Martino, A., Yan, C.-G., Li, Q., Denio, E., Castellanos, F., Alaerts, K., Anderson, J., Assaf, M., Bookheimer, S., Dapretto, M., Deen, B., Delmonte, S., Dinstein, I., Ertl-Wagner, B., Fair, D., Gallagher, L., Kennedy, D., Keown, C., Keysers, C., Lainhart, J., Lord, C., Luna, B., Menon, V., Minshew, N., Monk, C., Mueller, S., Müller, R.-A., Nebel, M., Nigg, J., O’Hearn, K., Pelphrey, K., Peltier, S., Sunaert, J. R. S., Thioux, M., Tyszka, J., Uddin, L., Wenderoth, J. V. N., Mostofsky, J. W. S., and Milham, M. (2014). The autism brain imaging data exchange: towards a large-scale evaluation of the intrinsic brain architecture in autism. *Molecular Psychiatry*, 19(6):659–667.
- Di Martino, A., Zuo, X.-N., Kelly, C., Grzadzinski, R., Mennes, M., Schvarcz, A., Rodman, J., Lord, C., Castellanos, F. X., , and Milham, M. P. (2013). Shared and distinct intrinsic functional network centrality in autism and attention-deficit/hyperactivity disorder. *Biological Psychiatry*, 74(8):623–632.
- Eidsvik, J., Shaby, B. A., Reich, B. J., Wheeler, M., and Niemi, J. (2014). Estimation and prediction in spatial models with block composite likelihoods. *Journal of Computational and Graphical Statistics*, 23(2):295–315.
- Finley, A. O., Datta, A., Cook, B. D., Morton, D. C., Andersen, H. E., and Banerjee, S. (2019). Efficient algorithms for Bayesian nearest neighbour Gaussian processes. *Journal of Computational and Graphical Statistics*, 28(2):401–414.

- Finley, A. O., Sang, H., Banerjee, S., and E.Gelfand, A. (2009). Improving the performance of predictive process modeling for large datasets. *Computational Statistics & Data Analysis*, 53(8):2873–2884.
- FMRIB Software Library (2018). FSL Atlases. <https://fsl.fmrib.ox.ac.uk/fsl/fslwiki/Atlases>. Last accessed on August 18, 2021.
- Fox, M. D. and Raichle, M. E. (2007). Spontaneous fluctuations in brain activity observed with functional magnetic resonance imaging. *Nature Reviews Neuroscience*, 8:700–711.
- Fuentes, M. (2007). Approximate likelihood for large irregularly spaced spatial data. *Journal of the American Statistical Association*, 102(477):321–331.
- Furrer, R., Bachoc, F., and Du, J. (2016). Asymptotic properties of multivariate tapering for estimation and prediction. *Journal of Multivariate Analysis*, 149:177–191.
- Furrer, R., Genton, M. G., and Nychka, D. W. (2006). Covariance tapering for interpolation of large spatial datasets. *Journal of Computational and Graphical Statistics*, 15(3):502–523.
- Genton, M. G. (2007). Separable approximations of space-time covariance matrices. *Environmetrics*, 18:681–695.
- Gneiting, T., , Genton, M. G., and Guttorp, P. (2007). *Statistics of Spatio-Temporal Systems*, chapter Geostatistical Space-Time Models, Stationarity, Separability and Full Symmetry, pages 151–175. Chapman & Hall.
- Godambe, V. P. (1991). *Estimating functions*. Oxford University Press.
- Ha, S., Sohn, I.-J., Kim, N., Sim, H. J., and Cheon, K.-A. (2015). Characteristics of brains in autism spectrum disorder: Structure, function and connectivity across the lifespan. *Experimental Neurobiology*, 24(4):273–284.
- Hansen, L. P. (1982). Large sample properties of generalized method of moments estimators. *Econometrica*, 50(4):1029–1054.
- Hansen, L. P., Heaton, J., and Yaron, A. (1996). Finite-sample properties of some alternative GMM estimators. *Journal of Business and Economic Statistics*, 14(3):262–280.
- He, Y., Wang, J., Wang, L., Chen, Z. J., Yan, C., Yang, H., Tang, H., Zhu, C., Gong, Q., Zang, Y., and Evans, A. C. (2009). Uncovering intrinsic modular organization of spontaneous brain activity in humans. *PLoS ONE*, 4(1):e5226.
- Heagerty, P. J. and Lele, S. (1998). A composite likelihood approach to binary spatial data. *Journal of the American Statistical Association*, 93(443):1099–1111.
- Heaton, M. J., Datta, A., Finley, A. O., Furrer, R., Guinness, J., Guhaniyogi, R., Gerber, F., Gramacy, R. B., Hammerling, D., Katzfuss, M., Lindgren, F., Nychka, D. W., Sun, F., and Zammit-Mangion, A. (2019). A case study competition among methods for analyzing large spatial data. *Journal of Agricultural, Biological and Environmental Statistics*, 24(398-425).

- Hector, E. C. and Reich, B. J. (2023). Distributed inference for spatial extremes modeling in high dimensions. *Journal of the American Statistical Association*, doi: 10.1080/01621459.2023.2186886.
- Hector, E. C. and Song, P. X.-K. (2020). Doubly distributed supervised learning and inference with high-dimensional correlated outcomes. *Journal of Machine Learning Research*, 21:1–35.
- Hector, E. C. and Song, P. X.-K. (2021). A distributed and integrated method of moments for high-dimensional correlated data analysis. *Journal of the American Statistical Association*, 116(534):805–818.
- Hector, E. C. and Song, P. X.-K. (2022). Joint integrative analysis of multiple data sources with correlated vector outcomes. *The Annals of Applied Statistics*, 16(3):1700–1717.
- Heyde, C. C. (1997). *Quasi-Likelihood and its Application: a General Approach to Optimal Parameter Estimation*. Springer Series in Statistics.
- Higdon, D. (2002). Space and space-time modeling using process convolutions. *Quantitative Methods for Current Environmental Issues*, pages 37–56.
- Jansiewicz, E. M., Goldber, M. C., Newschaffer, C. J., Denckla, M. B., Landa, R., and Mostofsky, S. H. (2006). Motor signs distinguish children with high functioning autism and asperger’s syndrome from controls. *Journal of autism and developmental disorders*, 36:613–621.
- Joe, H. and Lee, Y. (2009). On weighting of bivariate margins in pairwise likelihood. *Journal of Multivariate Analysis*, 100(4):670–685.
- Johannesson, G., Cressie, N., and Huang, H.-C. (2007). Dynamic multi-resolution spatial models. *Environmental and Ecological Statistics*, 14(1):5–25.
- Kang, E. L. and Cressie, N. A. (2011). Bayesian inference for the spatial random effects model. *Journal of the American Statistical Association*, 106(495):972–983.
- Katzfuss, M. (2017). A multi-resolution approximation for massive spatial datasets. *Journal of the American Statistical Association*, 112(517):201–214.
- Katzfuss, M. and Cressie, N. A. (2011). Spatio-temporal smoothing and em estimation for massive remote-sensing data sets. *Journal of Time Series Analysis*, 32:430–446.
- Katzfuss, M. and Gong, W. (2020). A class of multi-resolution approximations for large spatial datasets. *Statistica Sinica*.
- Kaufman, C. G., Schervish, M. J., and Nychka, D. W. (2008). Covariance tapering for likelihood-based estimation in large spatial data sets. *Journal of the American Statistical Association*, 103(484):1545–1555.
- Kuk, A. Y. and Nott, D. J. (2000). A pairwise likelihood approach to analyzing correlated binary data. *Statistics & Probability Letters*, 47(4):329–335.

- Kuk, A. Y. C. (2007). A hybrid pairwise likelihood method. *Biometrika*, 94(4):939–952.
- Lemos, R. T. and Sansó, B. (2009). A spatio-temporal model for mean, anomaly, and trend fields of north atlantic sea surface temperature. *Journal of the American Statistical Association*, 104(485):5–18.
- Li, Y. and Lin, X. (2006). Semiparametric normal transformation models for spatially ccorrelated survival data. *Journal of the American Statistical Association*, 101(474):591–603.
- Lindgren, F., Rue, H., and Lindström, J. (2011). An explicit link between gaussian fields and gaussian markov random fields: the stochastic partial differential equation approach. *Journal of the Royal Statistical Society, Series B*, 73(4):423–498.
- Lindsay, B. G. (1988). Composite likelihood methods. *Contemporary Mathematics*, 80:220–239.
- Liu, H., Ong, Y.-S., Shen, X., and Cai, J. (2020). When Gaussian process meets big data: A review of scalable GPs. *IEEE Transactions on Neural Networks and Learning Systems*, DOI: TNNLS.2019.2957109:1–19.
- Lynch, C. J., Uddin, L. Q., Supekar, K., Khouzam, A., Phillips, J., and Menon, V. (2013). Default mode network in childhood autism: posteromedial cortex heterogeneity and relationship with social deficits. *Biological Psychiatry*, 74(3):212–219.
- Manschot, C. and Hector, E. C. (2022). Functional regression with intensively measured longitudinal outcomes: a new lens through data partitioning. *arXiv*, arXiv:2207.13014.
- Nott, D. J. and Rydén, T. (1999). Pairwise likelihood methods for inference in image models. *Biometrika*, 86(3):661–676.
- Nychka, D. W., Bandyopadhyay, S., Hammerling, D., Lindgren, F., and Sain, S. (2015). A multiresolution Gaussian process model for the analysis of large spatial datasets. *Journal of Computational and Graphical Statistics*, 24(2):579–599.
- Rahko, J. S., Vuontela, V. A., Carlson, S., Nikkinen, J., Hurtig, T. M., Kuusikko-Gauffin, S., Mattila, M.-L., and Jukka J. Remes, K. K. J., Jansson-Verkasalo, E. M., Aronen, E. T., Pauls, D. L., Ebeling, H. E., Tervonen, O., Moilanen, I. K., and Kiviniemi, V. J. (2016). Attention and working memory in adolescents with autism spectrum disorder: a functional MRI study. *Child Psychiatry & Human Development*, 47(3):503–517.
- Rulli re, D., Durrande, N., Bachoc, F., and Cl (2018). Nested Kriging predictions for datasets with a large number of observations. *Statistics and Computing*, 28:849–867.
- Sang, H. and Huang, J. Z. (2012). A full scale approximation of covariance functions for large spatial data sets. *Journal of the Royal Statistical Society, Series B*, 74(1):111–132.
- Schabenberger, O. and Gotway, C. A. (2004). *Statistical methods for spatial data analysis*. Chapman & Hall.



- Stein, M. L. (2007). Spatial variation of total column ozone on a global scale. *The Annals of Applied Statistics*, 1(1):191–210.
- Stein, M. L. (2013). Statistical properties of covariance tapers. *Journal of Computational and Graphical Statistics*, 22(4):866–885.
- Stein, M. L., Chen, J., and Anitescu, M. (2013). Stochastic approximation of score functions for Gaussian processes. *The Annals of Applied Statistics*, 7(2):1162–1191.
- Stein, M. L., Chi, Z., and Welty, L. J. (2004). Approximating likelihoods for large spatial data sets. *Journal of the Royal Statistical Society, Series B*, 66(2):275–296.
- Sun, Y., Li, B., , and Genton, M. G. (2011). Geostatistics for large datasets. *Advances and Challenges in Space-time Modelling of Natural Events*, pages 55–77.
- Uddin, L. Q., Supekar, K., Lynch, C. J., Khouzam, A., Phillips, J., Feinstein, C., Ryali, S., and Menon, V. (2013). Salience network-based classification and prediction of symptom severity in children with autism. *Journal of the American Medical Association Psychiatry*, 70(8):869–879.
- Varin, C., Reid, N., and Firth, D. (2011). An overview of composite likelihood methods. *Statistica Sinica*, 21(1):5–42.
- Vecchia, A. V. (1988). Estimation and model identification for continuous spatial processes. *Journal of the Royal Statistical Society, Series B*, 50(2):297–312.
- Wang, J., Zuo, X., and He, Y. (2010). Graph-based network analysis of resting-state functional MRI. *Frontiers in Systems Neuroscience*, 4(16):1–14.
- Wolff, J. J., Jacob, S., and Ellison, J. T. (2018). The journey to autism: insights from neuroimaging studies of infants and toddlers. *Development and Psychopathology*, 30(2):479–495.
- Zhao, Y. and Joe, H. (2009). Composite likelihood estimation in multivariate data analysis. *The Canadian Journal of Statistics*, 33(3):335–356.
- Zimmerman, D. L. (1989). Computationally exploitable structure of covariance matrices and generalized covariance matrices in spatial models. *Journal of Statistical Computation and Simulation*, 32(1-2):1015.